# An experimental study on the onset of the horizontal convection

**Carlos Sanmiguel Vila[1,*], Tommaso Astarita[2], Giovanni Maria Carlomagno[2], Stefano Discetti[1], Andrea Ianiro[1]**

[1]Aerospace Engineering Group, University Carlos III of Madrid, Leganés, Spain
[2]Dipartimento di Ingegneria Industriale, Università degli Studi di Napoli Federico II, Napoli, Italy
*corresponding author: csanmigu@ing.uc3m.es

**Abstract** The convective phenomenology, driven by a differential heating along one horizontal boundary and commonly referred to as horizontal convection, is analyzed. The experimental apparatus consists of a polymethyl methacrylate parallelepiped box filled with water. Piecewise boundary conditions of uniform positive heat flux and constant temperature are imposed across the box length at its bottom wall. In fact, one half of the base has an uniform heat flux input condition realized with a printed circuit board heated by Joule effect; on the other half, a copper plate exists which is temperature conditioned by water passing through a serpentine brazed to it. The remainders of the box boundaries practically behave with adiabatic wall boundary conditions. An infrared camera is used to measure the temperature distribution on the outer side of the printed circuit board. The convective heat flux is extracted using the *heated thin-foil sensor* modified to account for the unsteady term of the energy balance. The experiments are carried out over a range of Rayleigh number $Ra_F$ (based on heat flux input and box length) from $1.3 \cdot 10^{11}$ to $1.1 \cdot 10^{12}$ and for a Prandtl number *Pr* (based on the initial water temperature) of approximately 7. Data are presented in terms of Nusselt number *Nu* distributions over the heated zone for several times after staring of heating. The measurement of the time-evolving *Nu* maps highlights the transition of the boundary layer and the onset and time evolution of the coherent structures. The onset of longitudinal rolls on the wall and the rise of a strong plume at the end wall are also shown.

**Keywords:** natural convection, infrared thermography, convection cells

## 1 Introduction

A fluid exposed to a variable heating condition along one horizontal boundary, such as a variation in temperature and/or heat flux, develops a circulation pattern of natural convective motion, which is known as horizontal convection [1]. Horizontal convection occurs in flows with paramount importance, such as the meridional overturning circulation in the oceans [2] where differential boundary conditions are provided on the ocean surface by the non-uniform solar radiation input, which is on average more intense at the Equator than at the poles. This occurrence has also an interest in other phenomena, such as the dynamics of the mantle of the Earth, and in industrial processes, such as glass/metal melting [3].
The dynamic features of this phenomenon are very different from the classic Rayleigh-Bernard configuration where the flow is heated from below and cooled from above [4]. In contrast to the Rayleigh-Bernard configuration where both boundaries promote an overturning of the fluid and there is a net heat transport between the boundaries, in horizontal convection, only one of the buoyancy sources is responsible of the overturning and, at steady state, there is no net heat flux through the boundary [5]. These particular features make the horizontal convection a peculiar and an intriguing problem. Nevertheless, horizontal convection has been less studied than the classic Rayleigh-Bénard problem, and still many questions remain at issue.
Along the possible boundary conditions to be imposed, one of the most investigated one is that where one side of the base has a given heat flux, while on the remaining part a fixed temperature condition is imposed. For its relative simplicity of experimental implementation, a uniform heating can be achieved in the portion of fixed heat flux conditions, while cooling is provided in the fixed temperature region. Under these circumstances, the flow is driven along the horizontal boundary, moving from the cold part towards the hot one to compensate for the vertical convective motion of the rising plume nearby the side wall contacting the heated zone. In fact, once the flow reaches the side wall, the flow rises in a large vertical plume adjacent to this wall. The convective cell is then closed by a horizontal flow region (involving large portions of the cell) and a sinking region on the sidewall opposite to that of the plume. For a more detailed description, the reader is referred to [5, 7]. A nice flow visualization is provided in Fig.1 (from [5]), where heating is applied on the left part of the bottom side of the box, while a fixed temperature condition is set on the right part of it.
The features of the flow motion are strongly dependent on the Rayleigh number (see in the following). At

low Rayleigh numbers, the motion is mainly driven by diffusion, and is stable in time while, above a critical Rayleigh number, the flow becomes unsteady as can be observed in the vicinity of the plume adjacent to the side wall [7].

Fig. 1 Horizontal convection in a thermally equilibrated laboratory experiment subject to heating and cooling that depends on position along the base of the box. Image taken from [5].

Some features of the horizontal convection, such as its initial transient, the governing dynamics of the thermal boundary layer or the transition to unsteady flow, have not been extensively studied. In the present paper, the objective of the investigation is to visualize the onset of horizontal convection. Experiments are carried out with infrared thermography, which provides a non-invasive measurement of the temperature distribution on the half of the base where the heat flux is provided. The convective heat transfer distribution is then inferred using an *unsteady version of the heated thin foil sensor* (as implemented in [6]). The influence of three different Rayleigh numbers is also discussed.

## 2 Experimental details

### 2.1 Parameters of the problem

The governing equations and an exhaustive analysis of the relevant dimensionless parameters of the problem are provided in [5, 7]. The main parameters governing the horizontal convection phenomena depend on the problem geometry, the working fluid and the boundary conditions.
The choice of the working fluid influences the Prandtl number:

$$Pr = \frac{\nu}{\kappa_T} \tag{1}$$

where $\kappa_T$ and $\nu$ are the thermal diffusivity and kinematic viscosity coefficient of the fluid, respectively.
The most relevant geometrical parameter of the domain is its aspect ratio:

$$A = \frac{H}{L} \tag{2}$$

where $H$ and $L$ are the height and the length of the domain, respectively.
The Rayleigh number, which is the ratio between buoyancy driven heat convection and heat diffusion, can be generally calculated as based on the imposed heat flux ($Ra_F$) or based on the imposed temperature difference ($Ra$), according to the boundary conditions nature of the problem to be studied. In the present work, because of the choice of uniform wall heat flux, the Rayleigh number is based on the imposed heat flux:

$$Ra_F = \frac{g\alpha F_T L^4}{\rho_0 c_f \kappa_T^2 \nu} \tag{3}$$

where $g$ is the gravity acceleration, $F_T$ is the input heat flux, $\alpha$ is the fluid thermal expansion coefficient, $\rho_0$ is the fluid density (measured at initial condition) and $c_f$ is the fluid specific heat. In the present study, the input heat flux is set so as to obtain $Ra_F$ equal to either $1.3 \cdot 10^{11}$, or $5 \cdot 10^{11}$, or $1.1 \cdot 10^{12}$; the Prandtl number is approximately equal to 7 and the aspect ratio $A$ is arranged equal to 0.5.
Since the present study is devoted to unsteady features of horizontal convection, a characteristic time scale must be chosen. The characteristic time of the thermal diffusion in the system is equal to $L^2/\kappa_T$. According to [7], in certain horizontal convection problems, the boundary layer thickness, which has to be considered as responsible of the heat transfer in the boundary layer, is of the order of $Ra_F^{-1/6} \cdot L$, thus in [11] it is

demonstrated that the characteristic time to reach steady temperature conditions in a fluid domain with horizontal convection is much smaller than the characteristic time of thermal diffusion and of the order of $L^2/\kappa_T \cdot Ra_F^{-1/6}$.
The object of the present investigation is the development of the horizontal convection flow features on the hot boundary, i.e. in the boundary layer region. The characteristic length to be chosen for the fluid thickness object of the present study has thus also to be of the order of $Ra_F^{-1/6} \cdot L$. As a consequence, it can be appropriate to define the characteristic time for the onset of the horizontal convection as:

$$t^* = \frac{L^2}{\kappa_T} \cdot Ra_F^{-1/3} \tag{4}$$

In practice, this short diffusive timescale should indicate how long it takes for the boundary layer to adjust to a new boundary condition [5,12].

### 2.2 Experimental apparatus

The conditions for horizontal convection are reproduced using a box filled with water. The box, which is sketched with the reference frame in figure 2, has internal dimensions of length $L = 300mm$, width $D = 150mm$, and height $H = 150mm$. The box is made of PlexiglasGS233. In order to minimize both the heat losses due to heat conduction towards the ambient and the tangential heat conduction through the walls, a wall thickness of 15mm has been chosen as a compromise value to assume adiabatic wall conditions.

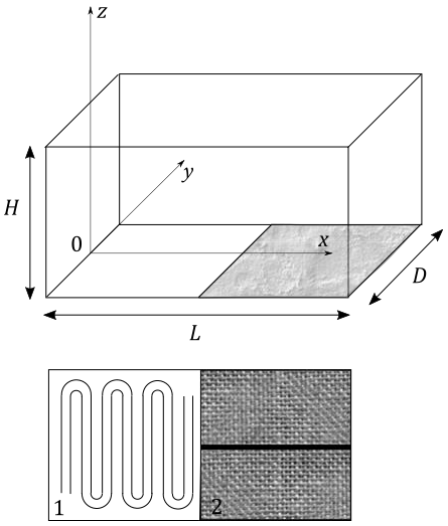


Fig. 2 Schematic view of the box with the reference frame. Below, a bottom view of the base where 1 is the copper serpentine and 2 is the printed board circuit with the structural reinforcement (black continuous line).

The base of the box is divided in two halves in order to obtain the desired piecewise boundary conditions of uniform heat flux input and constant temperature. The first half of the base (left) is a square electrolytic copper plate which has a side length of $150mm$ and thickness $s_{copper} = 10mm$, with a copper serpentine brazed below it. Water, kept at controlled temperature with a heat exchanger, passes through the serpentine and conditions the temperature of the copper plate. Considering usual values of the typical heat transfer coefficient $h$. The plate can be assumed as isothermal through its thickness because of the high thermal conductivity of the electrolytic copper ($\sim 390 Wm^{-1}K^{-1}$) which results in a low Biot number of the order of $10^{-2}$ over the entire plate ($Bi = hs_{copper}/\lambda_{copper}$, where $\lambda_{copper}$ is the thermal conductivity of the copper and $s_{copper}$ is the thickness of the copper plate). The serpentine ensures a constant (in time) and uniform (in space) temperature boundary condition on the inner plate wall, thus the copper plate can be assumed as at constant and uniform temperature throughout its volume, therefore adequately providing the desired boundary condition.
The second half of the base is a printed circuit board with nominal electrical resistance of $25.5\ \Omega$, wetted area $A_{circ} = 150x150mm^2$ and thickness $s_{circ} = 0.5mm$. The copper tracks of the circuit, oriented in the $y$ direction, are $5\mu m$ thick, $1.8mm$ wide and placed at a $2mm$ pitch. The circuit is heated by Joule effect using

a stabilized voltage power supply, thus providing a constant and uniform heat flux boundary condition. A structural reinforcement, visible in the plan view of Fig 2, is positioned in the center of the circuit oriented in the stream-wise direction to avoid bending and deformation of the board.

### 2.2 Heat transfer measurement

The temporal evolution of the local convective heat transfer coefficient $h$ on the printed circuit board side is recorded with an infrared (IR) camera in conjunction with the *unsteady heated thin foil heat flux sensor*.
The temperature of the printed circuit board is measured on its external side with a FLIR SC4000 IR camera. The circuit has been coated with a thin layer of high emissivity enamel ($\varepsilon = 0.95$) in order to improve the signal to noise ratio of the IR measurements. The characteristic Biot number of the printed circuit board ($Bi = hs_{circ}/\lambda_c$ , where $\lambda_c$ and $s_{circ}$ are the thermal conductivity and thickness of the circuit, respectively) and the inverse of the Fourier number ($Fo = \kappa_{circ}/fs_{circ}{}^2$, where $\kappa_{circ}$ is the thermal diffusivity of the circuit and $f$ is the IR sampling frequency rate) are small with respect to unity; consequently, both instantaneous and time-average temperatures can be considered constant through the printed circuit board thickness.
Applying a local unsteady energy balance to the circuit, the convective heat transfer coefficient $h$ can be evaluated as:

$$h = \frac{q_J - q_r - q_c - q_s}{T_w - T_{aw}} \tag{5}$$

where: $T_w$ is the wall temperature and $T_{aw}$ is the adiabatic wall temperature which coincides with the initial average temperature of the water in the box; $q_r$ is the radiation heat loss to the ambient, which can be estimated using the Stefan-Boltzmann's law,

$$q_r = \sigma\epsilon(T_w^4 - T_{amb}^4) \tag{6}$$

where $\sigma$ is the Stefan –Boltzmann's constant and $\varepsilon$ is the total hemispherical emissivity coefficient of the printed circuit board outer surface; $q_j$ is the Joule heat flux which is defined as $q_j = VI/A_{circ}$, where $V$ and $I$ are the electric voltage and current of the printed circuit board; $q_c$ is the thermal losses for tangential conduction which can be expressed according to [8] as,

$$q_c = s_{circ}\left(\lambda_{c,x}\frac{\partial^2 \mathrm{T}}{\partial \mathrm{x}^2} + \lambda_{c,y}\frac{\partial^2 \mathrm{T}}{\partial \mathrm{y}^2}\right) \tag{7}$$

where $\lambda_{c,x}$ and $\lambda_{c,y}$ are the thermal conductivities in the directions parallel and normal to the copper paths, respectively. The unsteady term $q_s$ is defined as

$$q_s = \rho_{circ}c_{circ}s_{circ}\frac{dT}{dt} \tag{8}$$

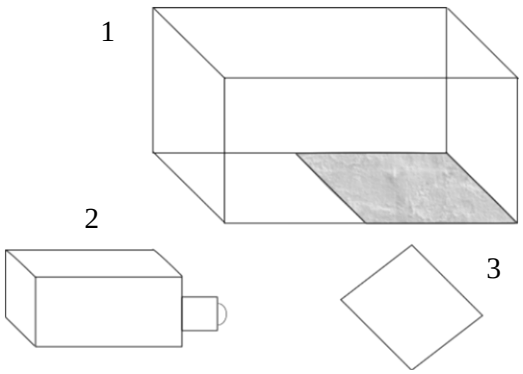


Fig. 3 Schematic view of the experimental setup. 1. Horizontal convection box; 2. IR camera; 3. First surface mirror.

where $\rho_{circ}$ and $c_{circ}$ are the average density and specific heat capacity of the circuit, respectively. Heat losses, due to natural convection effects on the external side of the box (to ambient), can be neglected.
The experimental procedure is detailed in the following. Initially, $T_{aw}$ is measured by averaging a set of images without providing electric current to the printed circuit board. Subsequently, the power supply is switched on and the horizontal convection regime is, therefore, triggered. Under these conditions, the sequence of $T_w$ images is measured and data reduced.
A sketch of the experimental measurement setup is reported in figure 3. A first surface mirror is placed in the optical path between the IR camera and the wall in order to enable an easy optical access. The spatial resolution achieved in the images is about 1*pix/mm*, with a noise equivalent temperature difference (NETD) of about $18mK$. The IR camera is calibrated by using a blackbody and reproducing the same optical path.
The correct measurement of the unsteady term in equation 5 requires highly accurate temperature measurements. The requirement set in [6]:

$$\frac{q_J - q_r - q_c}{\rho_{circ} c_{circ} s_{circ} f \cdot NETD} \gg 1 \qquad (9)$$

is satisfied for a sampling frequency rate $f$ = $4Hz$, which is the value chosen for the present experimental campaign. The image sequences are filtered with a 3D (space-time) Gaussian filter in order to reduce the effect of noise in the temperature measurements. The experimental data are reduced in dimensionless form in terms of Nusselt number, which is defined as $Nu = hL/k$, where $k$ is the thermal conductivity of the water.

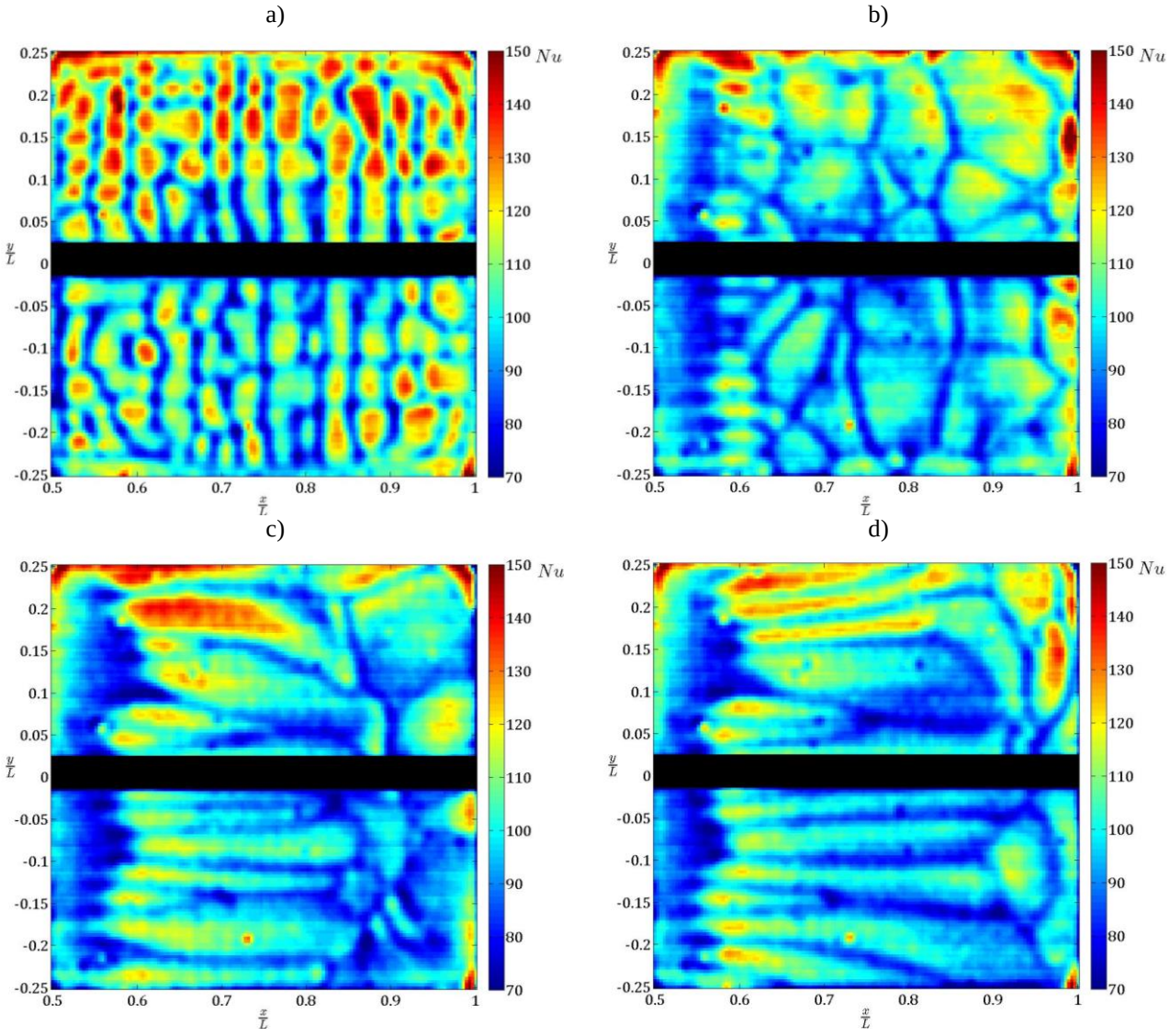


Fig. 4 Evolution of the $Nu$ distribution for $Ra_F = 1.3 \cdot 10^{11}$ measured at $t/t^*$: a) 0.3, b) 0.6, c) 1 and d) 2

## 3 Results

The onset of the horizontal convection and the development of the characteristic coherent structures are discussed in terms of the temporal evolution of the Nusselt number distribution on the half base where the heat flux is provided; in the maps, a black strip, oriented in the *x* direction, covers the region occupied by the structural reinforcement to the printed circuit board. The temporal evolution is reported for several non-dimensional times, normalized with respect to the characteristic time $t^*$ (Eq. 4).
Once the power supply is switched on, the electrical current starts to heat the printed circuit board. It can be observed the development of a spatially discontinuous distribution of the convective heat flux, which can be interpreted as the onset of a vertical convective motion in the form of local ascending plumes. This phenomenon is similar to the well know Rayleigh-Bénard *mushrooms*. The cells can be observed in Figs. 4a, 5a and 6a, where snapshots of the Nusselt number distribution are provided for the three different values of the Rayleigh number. It can be noticed that, the larger the Rayleigh number, the smaller the cells size, and that the average Nusselt number value tends to increase with increasing Rayleigh number. The orientation of the mushroom patterns, almost aligned in the *y* direction, may most probably be ascribed to the circuit tracks orientation (and the tiny gaps between them) even if their spatial frequency is much smaller.

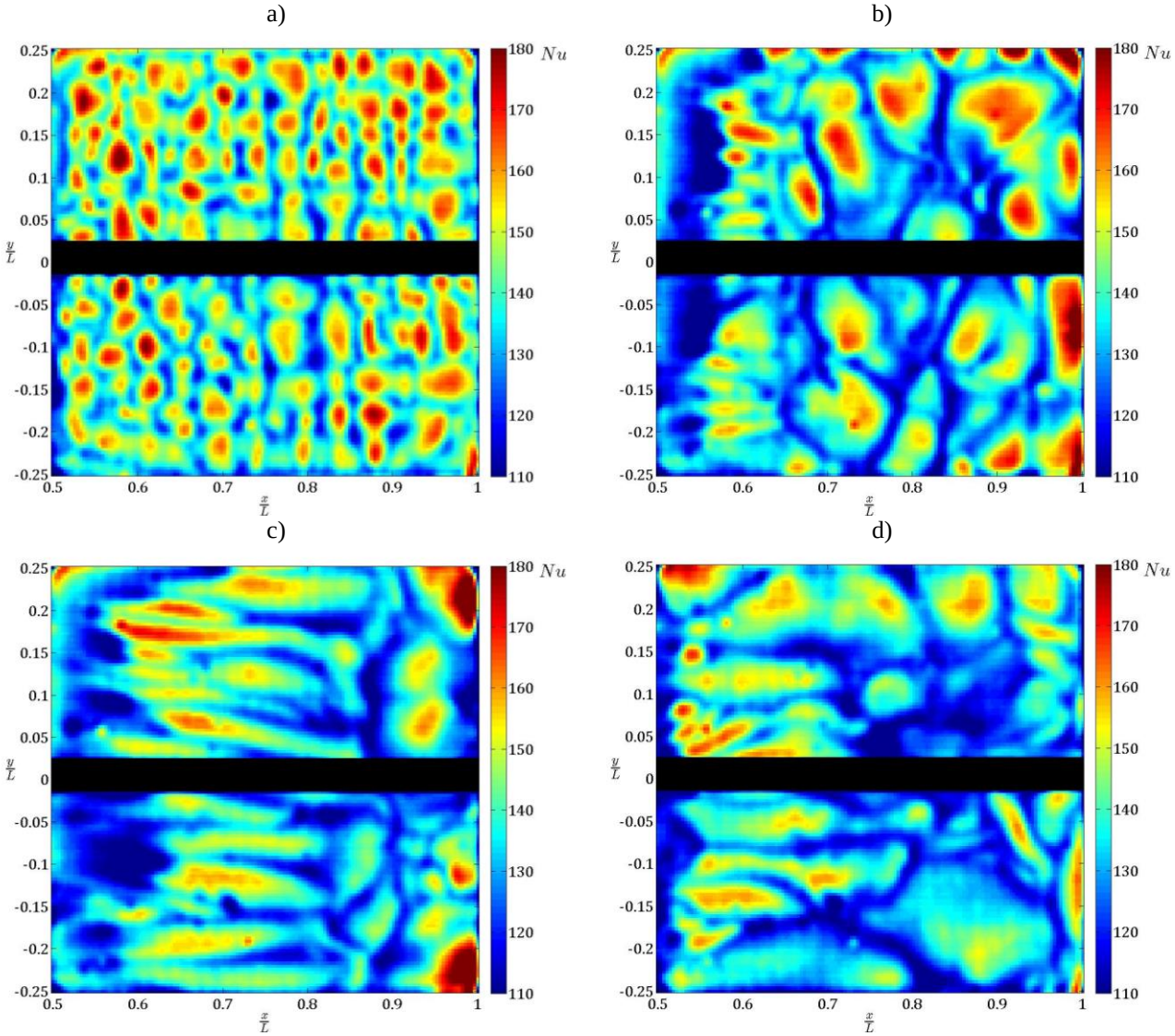


Fig. 5 Evolution of the $Nu$ distribution for $Ra_F = 5 \cdot 10^{11}$ measured after $t/t^*$: a) 0.3, b) 0.6, c) 1 and d) 2

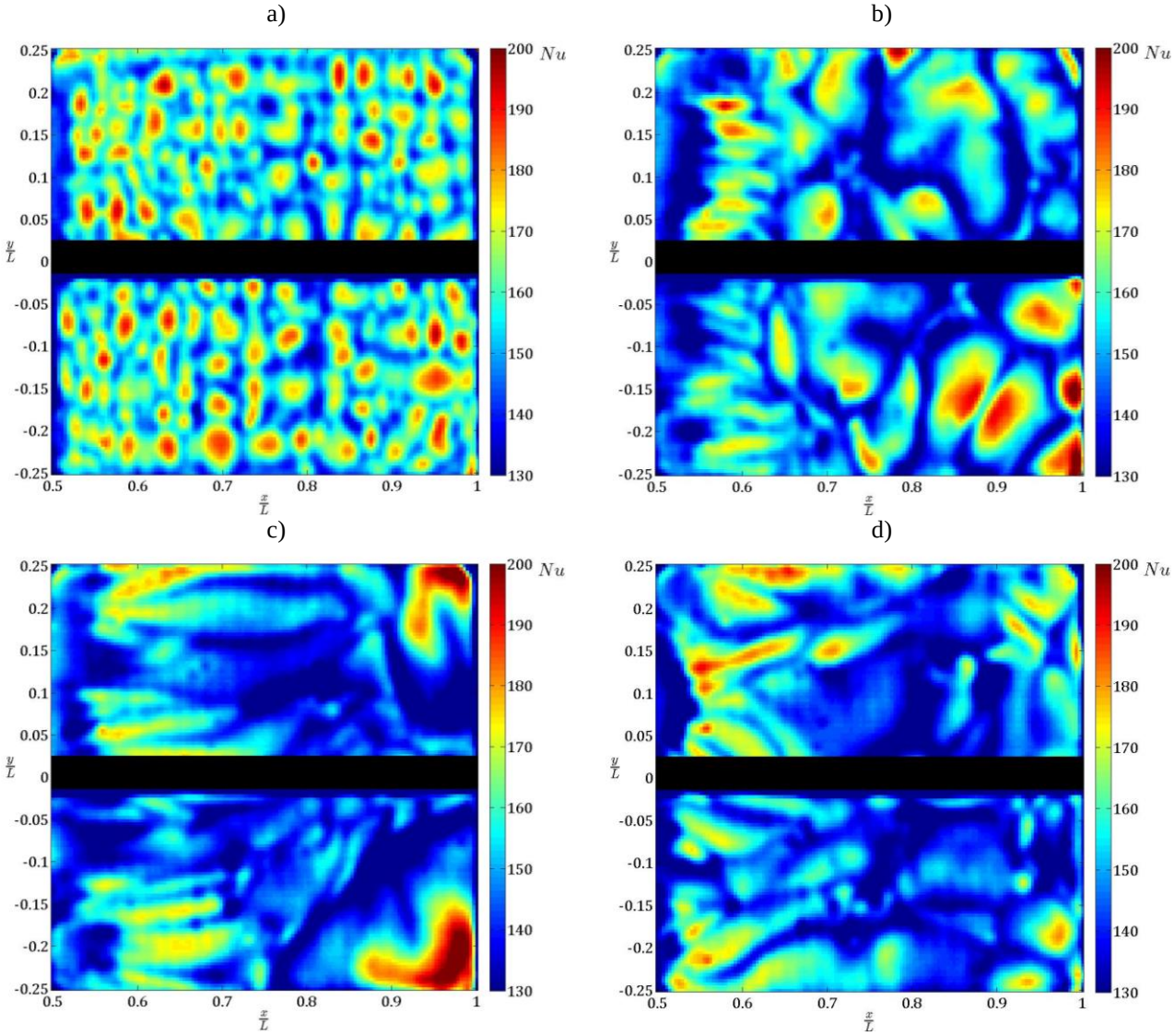


Fig. 6 Evolution of the $Nu$ distribution for $Ra_F = 1.1 \cdot 10^{12}$ measured after $t/t^*$: a) 0.3, b) 0.6, c) 1 and d) 2

In the first instant of the observation time, the field is dominated by the presence of these "Rayleigh-Bénard"-like cells. At the same time, due to the vertical mass flow rate in the ascending plumes, a horizontal mass flow rate of cold water is entrained towards the hottest regions to compensate for the fluid displaced in the vertical direction.

This results, first, in the cells coalescence (Figs. 4b, 5b, 6b) and, then, in the onset of a weak horizontal motion from the cold region to the hot region, which promotes the development of a boundary layer along the wall and tends to sweep out the vertical plumes (Figs. 4c, 5c, 6c).

Progressively, the penetration and intensity of the vertical plumes becomes weaker even if the vertical mass flow rates increases, as suggested by the observed more consistent boundary layer formed on the heat input region. When the horizontal motion is established, the lateral-directional instabilities determine the onset of longitudinal rolls. These rolls become the dominant structures (which replace the Rayleigh-Bénard cells) and are advected towards the end wall where merge in a macroscopic rising plume. In the horizontal convection literature, these rolls have been only mentioned in few studies [7, 9, 10]. In this stage of the transient (Figs. 4c, 5c, 6c), the distribution of the Nusselt number resembles that of a transitional boundary layer.

These rolls appear to be counter-rotating since in the down-wash section of each rolls pair, the heat transfer is increased and, in contrast, it is decreased in the upwash section. It can be observed that, when the Rayleigh number is increased, the rolls seem to generate a more turbulent flow. The rolls start at a certain location downstream of the beginning of the heat flux boundary; this transition may be ascribed to a laminar/turbulent

boundary layer transition since it seems to move forward with increasing Rayleigh number (Fig. 7).

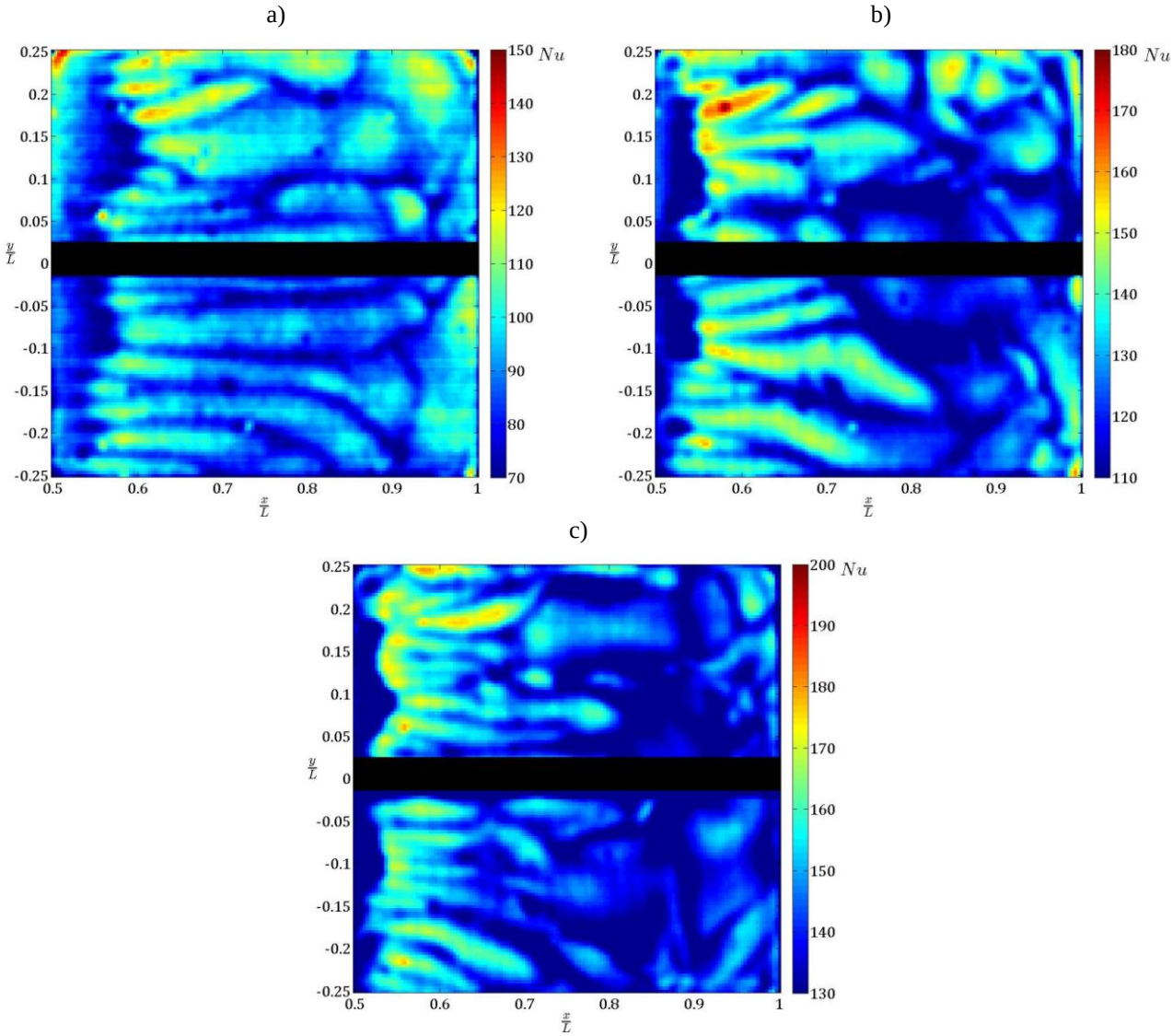


Fig. 7 $Nu$ distribution at $t/t^* = 6$ for: a) $Ra_F = 1.3 \cdot 10^{11}$, b)$Ra_F = 5 \cdot 10^{11}$, c) $Ra_F = 1.1 \cdot 10^{12}$

At $t/t^* = 2$, (Figs. 4d, 5d, 6d)., the vertical plumes are merged into the rolls and (towards the side wall) in a turbulent ascending plume which is one of the main characteristic aspects of horizontal convection. Because of this, a reduction of the longitudinal extension of the rolls can also be noted.
It has to be remarked that the development time of the characteristic flow features is strongly dependent on the Rayleigh number: the increase of $Ra_F$ increases the convective features. In all conditions, the time required to develop the horizontal convection is much smaller that the characteristic diffusion time and decreases with increasing $Ra_F$.
To confirm the appropriateness of the choice of the characteristic time $t^*$, Fig. 7 reports the $Nu$ distribution at $t/t^* = 6$, clearly showing similar $Nu$ patterns with respect to those at $t/t^* = 2$.

## 4 Conclusions

The onset of the horizontal convection phenomenon under boundary conditions of uniform heat flux input on one half of the domain base, and uniform temperature on the other half, is visualized using IR Thermography. The unsteady heated thin foil heat flux sensor has been implemented to obtain the temporal variation of the Nusselt distribution due to the unsteady features of the flow field under investigation.
The onset of the horizontal convection can be summarized in the following stages:

- initially the dominating flow features is the presence of "Rayleigh-Bénard" like mushrooms along the heated horizontal boundary;
- subsequently, as a result of the vertical mass flow, a weak horizontal motion is triggered which first makes these mushrooms to coalesce and then sucks fluid from the cold half of the base to the hot one;
- while the horizontal movement is established, longitudinal rolls begin to develop in the boundary layer with increasing streamwise extension along the heated boundary;
- finally, the horizontal flow sweeps away the Rayleigh-Bénard mushrooms and the horizontal rolls extend until the side wall where they separate and merge in a turbulent ascending plume.

The results have also shown that the higher the Rayleigh number is, the higher is the Nusselt number and the larger the turbulence of longitudinal rolls. The large temporal and spatial variations of the Nusselt number distribution reveal the leading role of the longitudinal rolls in determining the heat flux on the horizontal boundary.

The present work also allows to define a characteristic time for the development of the relevant flow features in horizontal convection, of the order of the diffusion characteristic time times $Ra_F^{-1/3}$. As demonstrated in [11], the time required to develop the horizontal convection is much smaller that the characteristic diffusion time; herein, it is shown that the onset of the convective flow is even smaller, corresponding to a decade for an ocean or to a couple of hours for a valley breeze.

**Acknowledgements**

The authors wish to thank the support of Carlos Cobos in the preparation of the experimental setup.

**References**

[1] Rossby, H. T. (1965). On thermal convection driven by non-uniform heating from below: an experimental study. In Deep Sea Research and Oceanographic Abstracts (Vol. 12, No. 1, pp. 9-16). Elsevier.
[2] Stern, M. E. (1975). Ocean circulation physics. New York: Academic
[3] Chiu-Webster, S., Hinch, E. J., & Lister, J. R. (2008). Very viscous horizontal convection. *Journal of Fluid Mechanics*, 611, 395-426.
[4] Bodenschatz, E., Pesch, W., & Ahlers, G. (2000). Recent developments in Rayleigh-Bénard convection. *Annual review of fluid mechanics*, 32(1), 709-778.
[5] Hughes, G. O., & Griffiths, R. W. (2008). Horizontal convection. *Annu. Rev. Fluid Mech.*, *40*, 185-208.
[6] Greco C S, Ianiro A, Cardone G (2014) Time and phase average heat transfer in single and twin circular synthetic impinging air jets. *International Journal of Heat and Mass Transfer*, vol. 73, pp 776-788. doi: 10.1016/j.ijheatmasstransfer.2014.02.030
[7] Mullarney, J. C., Griffiths, R. W., & Hughes, G. O. (2004). Convection driven by differential heating at a horizontal boundary. *Journal of Fluid Mechanics*, *516*, 181-209.
[8] Astarita, T., Cardone, G., & Carlomagno, G. M. (2006). Infrared thermography: An optical method in heat transfer and fluid flow visualisation. *Optics and lasers in engineering*, *44*(3), 261-281.
[9] Gayen, B., Griffiths, R. W., Hughes, G. O., & Saenz, J. A. (2013). Energetics of horizontal convection. Journal of Fluid Mechanics, 716, R10.
[10] Gayen, B., Griffiths, R. W., & Hughes, G. O. (2014). Stability transitions and turbulence in horizontal convection. *Journal of Fluid Mechanics*, *751*, 698-724.
[11] Griffiths, R. W., Hughes, G. O., & Gayen, B. (2013). Horizontal convection dynamics: insights from transient adjustment. *Journal of Fluid Mechanics*, 726, 559-595.
[12] Pierce, D. W., & Rhines, P. B. (1996). Convective building of a pycnocline: laboratory experiments. Journal of physical oceanography, 26(2), 176-190.